Clathrate nanostructures for mass spectrometry

Trent R. Northen[1,2]*, Oscar Yanes[1,2]*, Michael T. Northen[4], Dena Marrinucci[3], Winnie Uritboonthai[1,2], Junefredo Apon[1,2], Stephen L. Golledge[5], Anders Nordström[1,2] & Gary Siuzdak[1,2]*

The ability of mass spectrometry to generate intact biomolecular ions efficiently in the gas phase has led to its widespread application in metabolomics[1], proteomics[2], biological imaging[3], biomarker discovery[4] and clinical assays (namely neonatal screens[5]). Matrix-assisted laser desorption/ionization[6,7] (MALDI) and electrospray ionization[8] have been at the forefront of these developments. However, matrix application complicates the use of MALDI for cellular, tissue, biofluid and microarray analysis and can limit the spatial resolution because of the matrix crystal size[9] (typically more than 10 μm), sensitivity and detection of small compounds (less than 500 Da). Secondary-ion mass spectrometry[10] has extremely high lateral resolution (100 nm) and has found biological applications[11,12] although the energetic desorption/ionization is a limitation owing to molecular fragmentation. Here we introduce nanostructure-initiator mass spectrometry (NIMS), a tool for spatially defined mass analysis. NIMS uses 'initiator' molecules trapped in nanostructured surfaces or 'clathrates' to release and ionize intact molecules adsorbed on the surface. This surface responds to both ion and laser irradiation. The lateral resolution (ion-NIMS about 150 nm), sensitivity, matrix-free and reduced fragmentation of NIMS allows direct characterization of peptide microarrays, direct mass analysis of single cells, tissue imaging, and direct characterization of blood and urine.

A diagram of the main applications of NIMS is provided in Supplementary Fig. 1. Conceptually, NIMS reverses the system of desorption/ionization developed by Tanaka[7], which uses ~30-nm nanoparticles suspended in glycerol, where desorption/ionization is thought to occur by a thermally driven process for nanoparticles larger than 3 nm (ref. 13). As illustrated in Fig. 1a, b, NIMS uses a nanostructured surface composed of roughly 10-nm pores (Fig. 1c) to trap 'initiator' materials such as fluorinated siloxanes. The analyte is adsorbed on top of the NIMS surface and laser irradiation results in rapid surface heating causing initiator vaporization from many clathrates, triggering the desorption of adsorbed materials. Scanning electron microscopy (SEM) images of a laser-irradiated NIMS surface suggest that rapid surface heating results in a violent expansion of initiator, as indicated by bulk surface destruction and deformation (Fig. 1a). Ion irradiation also results in intact ion formation; however, SEM imaging (not shown) of ion-irradiated surfaces does not reveal any changes in surface nanostructure, indicating a more localized process. The large amounts of trapped initiators are found to migrate reversibly into and out of the NIMS surface with slight heating and cooling (Supplementary Movie 1), indicating that the initiator is highly ordered within the nanostructured surface. In these ways NIMS is very different from existing surface desorption/ionization techniques such as desorption–ionization on silicon[14] (DIOS), which is limited to small molecules and peptides, and laser

irradiation. In addition, NIMS is characterized by robustness, reproducibility, ease of preparation and minimal training for newcomers (Supplementary Methods), all of which have limited the application of DIOS.

NIMS is flexible as regards irradiation source, surface, and initiator composition: NIMS activity has been found to be compatible with a variety of irradiation including a nitrogen laser and ion sources (Au^+, Ga^+, Bi^+ and Bi_3^+). Native surfaces, silanized surfaces, and even surfaces sputtered with Au/Pd have NIMS activity. A wide range of initiators including lauric acid, polysiloxanes, siloxanes and silanes (molecular masses from 200 to 14,000 Da) have been used for NIMS (Supplementary Table 1), although the use of perfluorinated siloxanes was preferred for laser-NIMS because they are effectively trapped within the nanostructured surface and have the best performance, presumably as a result of the low solubility of analyte within the resulting clathrates. Because of the higher vacuum used
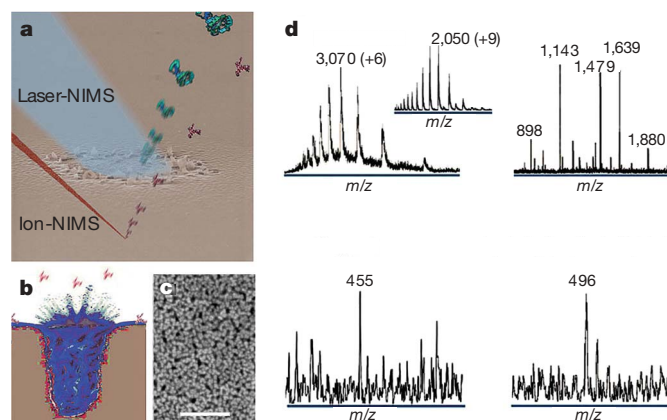

Figure 1 | Nanostructure-initiator mass spectrometry. a, Illustration superimposed on an SEM image of a NIMS surface after irradiation with a single laser shot (blue), revealing localized surface distortion and destruction. By comparison, ion irradiation (red) allows a much higher lateral resolution. **b**, Illustration of possible mechanism in which surface irradiation results in the vaporization or fragmentation of initiator (blue) trapped in a surface pore, triggering analyte desorption/ionization. **c**, SEM image revealing that the NIMS surface is composed of 10-nm pores. Scale bar, 100 nm. **d**, Laser irradiation (wavelength 337 nm) of a NIMS surface. Upper left panel: detection of a multiply charged protein (50 nmol of β-lactoglobulin) in a similar manner to ESI (inset). Upper right panel: detection of a BSA tryptic digest (500 amol). Lower left panel: detection of the calcium antagonist verapamil (700 ymol). Lower right panel: detection of the endogenous metabolite 1-palmitoyllysophosphatidylcholine (50 amol). The initiator was bis(tridecafluoro-1,1,2,2-tetrahydrooctyl)tetramethyl-disilazane; 0.5-μl drops were used. MALDI and ESI spectra for these samples are provided in Supplementary Figs 2, 3 and 5.

[1]Department of Molecular Biology, [2]Scripps Center for Mass Spectrometry, [3]Department of Cell Biology, The Scripps Research Institute, La Jolla, California 92037, USA. [4]Materials Department, University of California at Santa Barbara, Santa Barbara, California 93106, USA. [5]CAMCOR Surface Analysis Facility at the University of Oregon, Eugene, Oregon 97403, USA.
*These authors contributed equally to this work.

in time-of-flight–secondary-ion mass spectrometry (TOF–SIMS) instruments, a 14-kDa poly(3,3,3-trifluoropropylmethylsiloxanes) fluorinated siloxane was selected for ion-NIMS.

In contrast with recent approaches focused on altering the composition of the ion beam by using ion clustering[15], adding matrix[16], or Ag cationization[17] to generate intact ions, NIMS has taken advantage of the inherent properties of nanostructured surfaces, for example the ability to trap liquids or polymers and to absorb light, and their low thermoconductivity. Laser irradiation of NIMS surfaces results in the generation of intact ions derived from a wide range of biomolecules such as proteins, peptides, metabolites and drugs (Fig. 1d). Unlike conventional MALDI, laser-NIMS is capable of generating multiply charged proteins similarly to electrospray ionization (ESI)[8] and cryo-infrared MALDI[18] currently with best results for proteins with a molecular mass of less than 30 kDa (Supplementary Fig. 4). Comparison of NIMS and ESI spectra of identical samples (Fig. 1d) reveals that the charge distribution of the protein is shifted to higher charge states for ESI, indicating that the protein is not as denatured by NIMS or possibly loses some charge during the ionization process. The inherent properties of nanostructured surfaces are also reflected in the higher sensitivity than with ESI and MALDI (Fig. 1d and Supplementary Figs 2, 3 and 5). Figure 1d shows the detection of 700 ymol of verapamil (a calcium antagonist drug) and a peptide mass fingerprint of 500 amol of bovine serum albumin, resulting in 55% sequence coverage. Taking advantage of the sensitivity of laser-NIMS it was possible to desorb/ionize endogenous phospholipids from few cells or even a single cell (Fig. 2 and Supplementary Discussion) of a highly metastatic breast cancer cell line (MDA-MB-231) with superior complexity than was achieved with hundreds of cells by nanoESI, MALDI or ion-NIMS.

The high lateral resolution (about 150 nm), reduced fragmentation, and sensitivity of ion-NIMS allow the direct characterization of peptide microarrays. In situ mass spectrometry enables label-free characterization of arrays and may eventually allow the analysis of biomolecules bound to the arrays from complex mixtures such as serum. Given the small feature size of current microarray

technologies (10 μm)[19], high-lateral-resolution analysis with SIMS is desirable; however, the fragmentation complicates identification[20]. Using ion-NIMS for high-resolution label-free analysis of a peptide array resulted in mass spectra and mass images obtained at 1 fmol of peptide (Fig. 3a, b), which is a 1,000-fold enhancement in sensitivity over other TOF–SIMS strategies for intact biomolecules[16,21] and doubles the mass range for peptide analysis with cluster sources[15]. This improvement in molecular ion sensitivity is probably due to a decrease in fragmentation typical of TOF–SIMS seen in identical samples spotted on a silicon control surface (Fig. 3d). The high resolution of NIMS revealed that bradykinin peptides localize themselves at the centre of the printed spot in depositions of higher concentration (Fig. 3c). However, because ion-NIMS is a surface effect, it may not be suitable for depth profiling experiments.

Unlike existing mass spectrometry imaging methods, which desorb/ionize molecules from the tissue surface[9,22], the NIMS surface permits the imaging of metabolites at the tissue/surface interface as shown in Fig. 4a. The initial step is ablation of the surface tissue with high laser energies (about 0.4 J cm^{-2} per pulse) followed by direct interrogation of the tissue/surface interface with lower-energy laser irradiation (about 0.01 J cm^{-2} per pulse) for mass spectral imaging (Fig. 4a). NIMS analysis of mouse embryo tissue sections reveals complex and different ion profiles between developing tissue types; some of these ions have been identified as lipids by using post-source decay because of their labile headgroups, for example phosphatidylcholine and phosphatidylethanolamine (Fig. 4, Supplementary Fig. 6 and Supplementary Table 2), whereas TOF/TOF or Fourier-transform mass spectrometry instrumentation should further enable the identification of other classes of metabolite. The high intensity of these phospholipids is attributed to both the high concentration of these species in biological membranes and the efficient partitioning of these metabolites onto the fluorinated clathrates (for example, bis(heptadecafluoro-1,1,2,2-tetrahydrodecyl)tetramethyl-disiloxane) and not as a result of greater sensitivity of NIMS for lipids
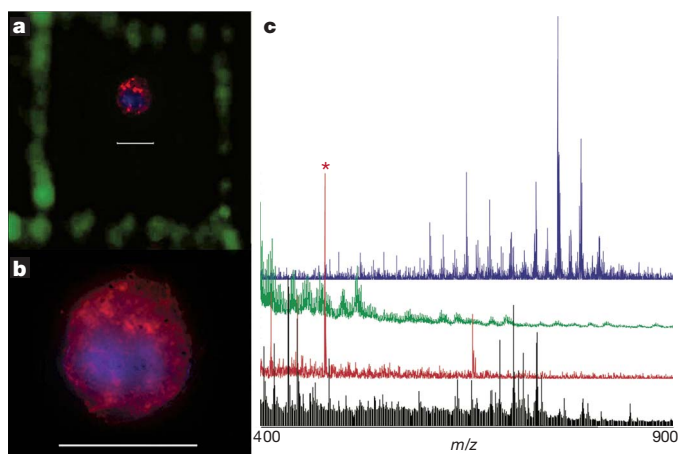

Figure 2 | Laser-NIMS and fluorescent analysis of a single cancer cell.
a, Fluorescent image of a MDA-MB-231 cancer cell after laser-NIMS analysis, fixing with paraformaldehyde, permeabilization with methanol, and staining with both 4,6-diamidino-2-phenylindole (blue) and Alexa 555-cytokeratin antibodies (red). The cell's location is indicated by being surrounded by a green fluorescent box formed with the same laser as that used for mass analysis at high intensity. b, Higher-resolution fluorescent image of the cell. c, Mass spectra from the cell with the use of laser-NIMS (blue) compared with 100 cells measured with ion-NIMS (green), MALDI analysis of 400 cells (red), and 500 cells measured with nanoelectrospray ionization (black). Laser-NIMS spectra were performed with bis(tridecafluoro-1,1,2,2-tetrahydrooctyl)tetramethyl-disiloxane initiator calibrated with Na$^+$, K$^+$, phosphocholine and 1-palmitoyllysophosphatidylcholine. Scale bar, 28 μm. Asterisk, matrix background ion.
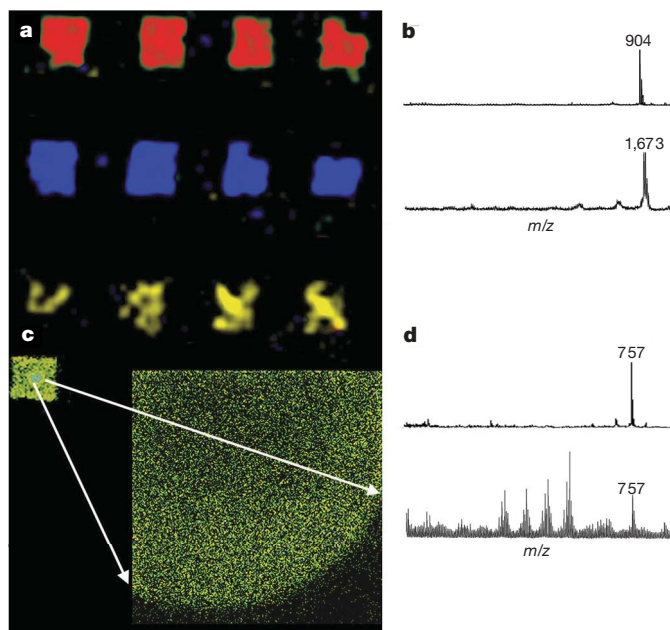

Figure 3 | Bi$_3^+$ ion imaging of peptide array on ion-NIMS surface.
a, Selective ion image of peptide array showing the localization of bradykinin 2-9 (red), neurotensin (blue) and bradykinin 1-7 (yellow) at 1 fmol. b, Corresponding mass spectra of bradykinin 2-9 (904 Da) and neurotensin (1,673 Da) at 1 fmol. c, Ion-NIMS mass spectrum of bradykinin 1-7 at 1 pmol revealing the localization of peptide in the centre of the spot as shown (inset) with a high-resolution image (150-nm ion beam). d, Bradykinin 1-7 (757 Da) also shown at 1 pmol both off the NIMS surface (top) and a silicon control surface, the latter showing significant fragmentation.
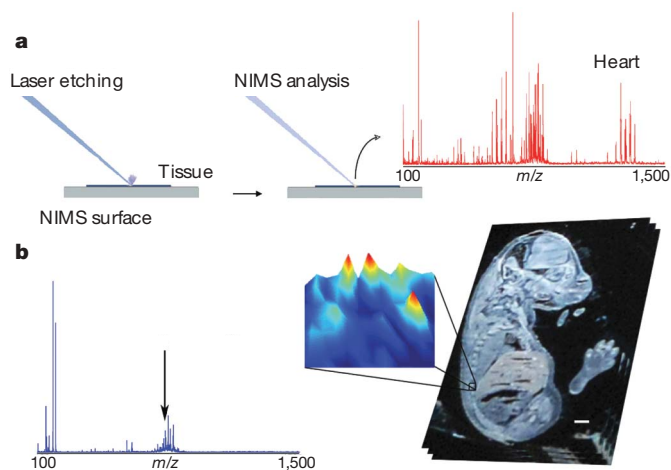
Figure 4 | Tissue imaging by laser-NIMS. a, The concept of tissue mass profiling: tissue slices (sections about 12 μm thick from a mouse embryo) on the NIMS surface are etched with high laser energies (about 0.4 J cm^{-2} per pulse), exposing the underlying surface. Laser irradiation (about 0.01 J cm^{-2} per pulse) of the 'etched' area results in desorption/ionization of metabolites, for example in developing heart tissue. **b,** Mass spectrometry imaging of glycerophosphatidylcholine (*m/z* 782, arrow) localized around a developing vertebra from a mouse embryo section (right). The resulting 300-μm-wide false-colour mass intensity image (inset) reveals a higher intensity (red, yellow and cyan) surrounding the developing vertebra (dark blue). The photograph is of the unstained section on the NIMS surface before analysis. The initiator was bis(heptadecafluoro-1,1,2,2-tetrahydrodecyl)tetramethyl-disiloxane and imaging was performed with a 20-μm step size by using a laser beam about 15 μm in diameter. Scale bar, 1 mm.

(Supplementary Fig. 7). In addition, changing to non-fluorous initiators changes the ion profiles markedly (Supplementary Fig. 8). Anatomical features are clearly visible, facilitating imaging of the developing vertebra, revealing the localization of the lipids around the developing bone (Fig. 4b and Supplementary Fig. 9), and the NIMS surface maintains metabolite localization on this length scale (about 50 μm). Overall, NIMS is well suited for imaging metabolites from tissues; in this it is complementary to MALDI, which is better suited to the detection of peptides and small proteins in tissue samples[23].

NIMS allows direct analysis (no sample preparation) of submicrolitre sample volumes of blood and urine, resulting in complex spectra without background ions (Fig. 5). This is in contrast with existing mass spectrometry approaches to biofluid analysis such as liquid chromatography (LC)–ESI, which requires extraction[24,25], and gas chromatography–mass spectrometry, which typically requires both extraction and derivatization[25]. Although MALDI can be used directly (a comparison of NIMS with MALDI is given in Supplementary Figs 10 and 11), fractionation and/or desalting are typically required to obtain good matrix–analyte co-crystallization[26,27]. Consistent with analysis of cells and tissues is the observation that lipids from blood effectively partition onto and ionize from perfluorinated bis(heptadecafluoro-1,1,2,2-tetrahydrodecyl)tetramethyl-disiloxane) clathrates. In contrast, urine spectra are largely dominated by small metabolites (less than 500 Da), although larger metabolites (such as putative gangliosides GM2 and GM1, with *m/z* 1545.9 and 1561.9, respectively) are also detected. Switching to a more polar hydroxylated siloxane initiator results in a markedly different ion profile, in which about 86% of the ions are unique to the perfluorinated surface. This suggests that initiator selection can be used to target metabolites on the basis of physical and chemical functionalities. In addition, because the concentration of metabolites is often critical in clinical assays, it is important to note that NIMS analysis is capable of detecting metabolites (in this case, codeine) quantitatively from urine at low levels (Fig. 5 inset; linear response until 15 ng ml^{-1}), in contrast with 75–250 ng ml^{-1} obtainable with the conventional approaches[28].
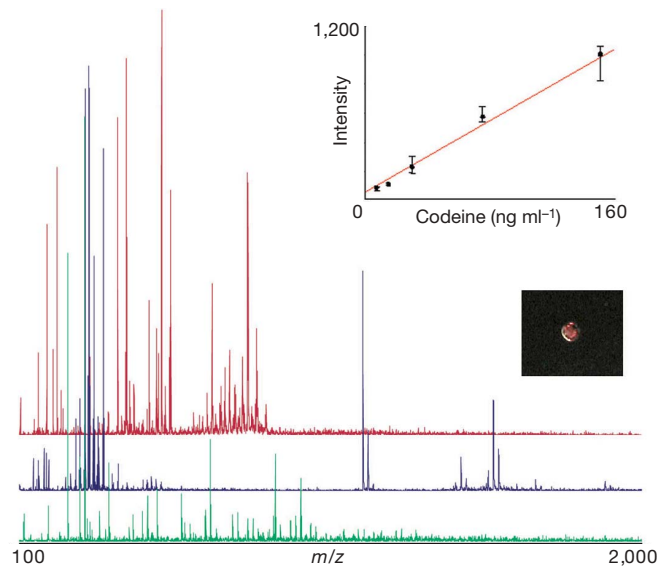

Figure 5 | Direct analysis of biofluids by laser-NIMS without sample preparation. Mass spectra of fresh blood (1 μl) obtained after laser etching (red) and urine (1 μl) (blue) with the use of bis(heptadecafluoro-1,1,2,2-tetrahydrodecyl)tetramethyl-disiloxane initiator. A markedly different spectrum (green) is obtained from the same urine by changing the initiator to 1,3-bis(hydroxybutyl)tetramethyldisiloxane. Inset: quantitative analysis of urine sample spiked with different concentrations of codeine shows a linear response up to 15 ng ml^{-1}, indicating that NIMS is suitable for metabolite quantification. Error bars represent s.d.

NIMS affords many possible applications and challenges: currently, our efforts are focused on interfacing NIMS with Fourier-transform mass spectrometry to improve metabolite identification on tissues, as well as immobilizing ligands on the NIMS surface for screening metabolite interactions and enzymatic activities. NIMS can also be developed for biomedical applications such as fundamental studies on single cells, developing high-throughput clinical tests, and conducting studies on pharmacokinetics and drug localization in tissues. The primary challenges include broadening the scope of NIMS through the use of new initiators, ideally including reactive initiators for direct chemical derivatization, and creating nanostructured surfaces to enhance desorption/ionization.

METHODS SUMMARY

Animal welfare. All procedures involving mice were approved by the Institutional Animal Care and Use Committee at Scripps Research Institute and conform to National Institutes of Health guidelines and public law.

Preparation of NIMS surfaces. Low-resistivity (0.01–0.02 Ω cm) P-type ⟨100⟩ (boron) silicon was etched at 48 mA cm^{-2} for 30 min. Various initiators were used on both silanized and unsilanized surfaces (Supplementary Information). For laser-NIMS, undiluted initiator solution was applied at room temperature (25 °C) for 30–60 min to the surface, and excess initiator was removed with a jet of nitrogen. For ion-NIMS, a 14-kDa poly(3,3,3-trifluoropropylmethylsiloxanes) polymer was applied to a silanized and vacuum-baked surface, then baked overnight at 100 °C; excess polymer was removed with a jet of nitrogen and brief rinsing with tert-butyl methyl ether.

Additional details are given in Supplementary Movies 2–8 and additional illustrated procedures in Supplementary Information.

Sample preparation. Peptides were printed by using robotic contact printing (1.4-nl drops). MDA-MB-231 cells were deposited on the NIMS surface with a micromanipulator, and after mass spectrometry analysis they were fixed and permeabilized, stained immunofluorescently and imaged. Embryos were collected, quickly frozen in OCT compound (VWR International), sectioned (12-μm slices) and then thaw-mounted on a NIMS chip. Fresh urine or blood samples were spotted directly on the NIMS surface and the excess was blown off with nitrogen. Urine samples were analysed directly and blood was first laser etched (see Fig. 5).

1. Want, E. J., Cravatt, B. F. & Siuzdak, G. The expanding role of mass spectrometry in metabolite profiling and characterization. *ChemBioChem* **6,** 1941–1951 (2005).
2. Aebersold, R. & Mann, M. Mass spectrometry-based proteomics. *Nature* **422,** 198–207 (2003).
3. Chaurand, P., Stoeckli, M. & Caprioli, R. M. Direct profiling of proteins in biological tissue sections by MALDI mass spectrometry. *Anal. Chem.* **71,** 5263–5270 (1999).
4. Lindon, J. C., Holmes, E. & Nicholson, J. K. Metabonomics in pharmaceutical R&D. *FEBS J.* **274,** 1140–1151 (2007).
5. Chace, D. H. *et al.* Rapid diagnosis of phenylketonuria by quantitative analysis for phenylalanine and tyrosine in neonatal blood spots by tandem mass spectrometry. *Clin. Chem.* **39,** 66–71 (1993).
6. Karas, M. & Hillenkamp, F. Laser desorption ionization of proteins with molecular masses exceeding 10,000 daltons. *Anal. Chem.* **60,** 2299–2301 (1988).
7. Tanaka, K. *et al.* Protein and polymer analyses up to *m/z* 100 000 by laser ionization time of flight mass spectrometry. *Rapid Commun. Mass Spectrom.* **2,** 151–153 (1988).
8. Fenn, J. B., Mann, M., Meng, C. K., Wong, S. F. & Whitehouse, C. M. Electrospray ionization for mass spectrometry of large biomolecules. *Science* **246,** 64–71 (1989).
9. Caldwell, R. L. & Caprioli, R. M. Tissue profiling by mass spectrometry: a review of methodology and applications. *Mol. Cell. Proteomics* **4,** 394–401 (2005).
10. Benninghoven, A. in *Secondary Ion Mass Spectrometry* (eds Benninghoven, A., Rüdenauer, F. G. & Werner, H. W.) 1–6, 664–761 (Wiley, New York, 1987).
11. Kraft, M. L., Weber, P. K., Longo, M. L., Hutcheon, I. D. & Boxer, S. G. Phase separation of lipid membranes analyzed with high-resolution secondary ion mass spectrometry. *Science* **313,** 1948–1951 (2006).
12. Ostrowski, S. G. *et al.* Secondary ion MS imaging of lipids in picoliter vials with a buckminsterfullerene ion source. *Anal. Chem.* **77,** 6190–6196 (2005).
13. McLean, J. A., Stumpo, K. A. & Russell, D. H. Size-selected (2–10 nm) gold nanoparticles for matrix assisted laser desorption ionization of peptides. *J. Am. Chem. Soc.* **127,** 5304–5305 (2005).
14. Wei, J., Buriak, J. M. & Siuzdak, G. Desorption–ionization mass spectrometry on porous silicon. *Nature* **399,** 243–246 (1999).
15. Winograd, N. The magic of cluster SIMS. *Anal. Chem.* **77,** 142A–149A (2005).
16. Wu, K. J. & Odom, R. W. Matrix-enhanced secondary ion mass spectrometry: A method for molecular analysis of solid surfaces. *Anal. Chem.* **68,** 873–882 (1996).
17. Grade, H. & Cooks, R. G. Secondary ion mass-spectrometry—cationization of organic-molecules with metals. *J. Am. Chem. Soc.* **100,** 5615–5621 (1978).
18. Overberg, A., Karas, M., Bahr, U., Kaufmann, R. & Hillenkamp, F. Matrix-assisted infrared-laser (2.94-μm) desorption ionization mass-spectrometry of large biomolecules. *Rapid Commun. Mass Spectrom.* **4,** 293–296 (1990).
19. Singh-Gasson, S. *et al.* Maskless fabrication of light-directed oligonucleotide microarrays using a digital micromirror array. *Nature Biotechnol.* **17,** 974–978 (1999).
20. Hashimoto, H., Nakamura, K., Takase, H., Okamoto, T. & Yamamoto, N. Quantitative TOF-SIMS imaging of DNA microarrays produced by bubble jet printing technique and the role of TOF-SIMS in life science industry. *Appl. Surf. Sci.* **231–2,** 385–391 (2004).
21. Xu, J. Y., Braun, R. M. & Winograd, N. Applicability of imaging time-of flight secondary ion MS to the characterization of solid-phase synthesized combinatorial libraries. *Anal. Chem.* **75,** 6155–6162 (2003).
22. Wiseman, J. M., Ifa, D. R., Song, Q. & Cooks, R. G. Tissue imaging at atmospheric pressure using desorption electrospray ionization (DESI) mass spectrometry. *Angew. Chem. Int. Edn Engl.* **45,** 7188–7192 (2006).
23. Chaurand, P., Norris, J. L., Cornett, D. S., Mobley, J. A. & Caprioli, R. M. New developments in profiling and imaging of proteins from tissue sections by MALDI mass spectrometry. *J. Proteome Res.* **5,** 2889–2900 (2006).
24. Hao, C., Clement, R. & Yang, P. Liquid chromatography–tandem mass spectrometry of bioactive pharmaceutical compounds in the aquatic environment—a decade's activities. *Anal. Bioanal. Chem.* **387,** 1247–1257 (2007).
25. Maurer, H. H. Position of chromatographic techniques in screening for detection of drugs or poisons in clinical and forensic toxicology and/or doping control. *Clin. Chem. Lab. Med.* **42,** 1310–1324 (2004).
26. Fiedler, G. M. *et al.* Standardized peptidome profiling of human urine by magnetic bead separation and matrix-assisted laser desorption/ionization time-of-flight mass spectrometry. *Clin. Chem.* **53,** 421–428 (2007).
27. Villanueva, J. *et al.* Serum peptide profiling by magnetic particle-assisted, automated sample processing and MALDI-TOF mass spectrometry. *Anal. Chem.* **76,** 1560–1570 (2004).
28. Kraemer, T. & Paul, L. D. Bioanalytical procedures for determination of drugs of abuse in blood. *Anal. Bioanal. Chem.* **388,** 1415–1435 (2007).

Author Contributions T.R.N. and O.Y. contributed equally to this work. T.R.N. and G.S. conceived of NIMS, developed and applied NIMS, designed experiments, analysed data, and wrote the manuscript. O.Y. developed and applied NIMS, designed experiments, analysed data, and wrote the manuscript. M.T.N. performed SEM studies. D.M. prepared cell cultures and performed fluorescent imaging. A.N. and W.U. developed and applied NIMS. J.A. used NIMS to image mouse embryo. S.L.G. performed ion-NIMS.

METHODS

Materials. Hydrofluoric acid, ethanol, trifluoracetic acid, trichloroacetic acid, acetonitrile and methanol were purchased from Fisher Scientific and were of the highest purity available. All silanes and siloxanes were purchased from Gelest. Single-side-polished silicon wafers, P/boron-type, ⟨100⟩ orientation, low resistivity (0.01–0.02 Ω cm), $525 \pm 25\,\mu m$ thick and 100 mm in diameter, were obtained from Silicon Valley Microelectronics. Bovine serum albumin (BSA), thymopoietin II, sinapic acid, α-cyano-4-hydroxycinnamic acid, dithiothreitol, tert-butyl methyl ether, iodoacetamide, verapamil, β-lactoglobulin, 1-palmitoyllysophosphatidylcholine, neurotensin, bradykinin 1-7 and bradykinin 2-9 were from Sigma-Aldrich. Mass spectrometry grade porcine trypsin was from Promega. Bacteriorhodopsin was a gift from V.-P. Jaakola and R. C. Stevens. Fresh blood and urine from humans were used in this study. Amphetamine, methamphetamine, morphine, benzoylecgonine and codeine were gifts from R. L. Fitzgerald and D. Herold.

Instrumentation. An etching chamber was constructed in house and current was provided with a Bio-Rad PowerPack1000 (see details at http://masspec.scripps.edu/Research/nims/create.php). MDA-MB-231 cells (ATCC HTB-26) were grown at 37 °C in Leibovitz's L-15 medium with 2 mM L-glutamine and 10% calf bovine serum, then harvested from growth flasks by treatment with trypsin-EDTA. Human AB serum (Sigma) was used to block the surface prior to incubation with a mouse monoclonal anti-Pan cytokeratin antibody (Sigma) which was followed by incubation with Alexa555 goat anti-mouse antibody (Invitrogen) and 4,6-diamidino-2-phenylindole (DAPI) nuclear counterstain (Invitrogen).

Scanning electron microscopy images were collected on native (SiH) and NIMS surfaces coated with about 3 nm of Au/Pd with a Sirion FEG Digital Scanning Microscope (FEI Company). Laser-NIMS and MALDI were performed with a VoyagerDE STR (Applied Biosystems) equipped with delay extraction (DE) and a 337-nm pulsed nitrogen laser. Ion-NIMS was performed with ION-TOF IV TOF–SIMS (IONTOF GmbH) with a polyatomic Bi^+ source. An Agilent 1100 series LC–ESI-TOF was used for model compound analysis with direct infusion. BSA digest and cancer cell analysis were performed with a ThermoFinnigan LTQ linear ion trap fitted with a custom nanoelectrospray source (2 kV at the tip).

A micromanipulator (MINJ-PD; Tritech Research) was used to precisely count and expel cells onto the NIMS substrate, MALDI plate and Eppendorf tubes (nanoLC–ESI analysis). Cells were dried and mass spectral analysis was completed. Fluorescent imaging was performed with a Nikon TE2000 fluorescent microscope with an automated stage; a 20× Plan Fluor (numerical aperture (NA) 0.45) objective was used for initial image acquisition and a 60× oil Plan Apo (NA 1.40) objective for higher-resolution imaging. The microscope had automated excitation and emission filter wheels (Lamda 10-2; Sutter Instrument) with a triple band filter set for DAPI, fluorescein isothiocyanate and tetramethyl rhodamine isothiocyanate (61000V2; Chroma Technology Corp.). Digital images were acquired through a Retiga EXi Fast 1394 Mono Cooled digital camera (Qimaging).

Embryo tissue sections were prepared by cryosectioning with a Leica CM3050 S cryostat to a thickness of 12 μm, and then thaw-mounted directly onto a NIMS chip.

Preparation of nanostructured silicon. Nanostructured silicon was prepared, with extreme caution, by using anodic etching in 25% hydrofluoric acid in ethanol. A current density of $48\,mA\,cm^{-2}$ was applied for 30 min. After etching, undiluted initiator was applied at room temperature for 30–60 min on both silanized or unsilanized surfaces. Excess polymer was removed by using a jet of nitrogen (see more details at Supplementary Methods and http://masspec.scripps.edu/Research/nims/create.php for a step-by-step procedure). For laser-NIMS, different siloxane compounds were used as initiators (see Supplementary Table 1) and for ion-NIMS 14-kDa poly(3,3,3-trifluoropropylmethylsiloxanes) polymer was applied to the surface and baked overnight at 100 °C; excess polymer was removed with a jet of nitrogen and brief dropwise rinsing with tert-butyl methyl ether.

Mass spectrometry. Laser-NIMS and MALDI: samples (for example, tissue slices) were revealed in the mass spectrometer by using a charge-coupled device camera. Each recorded mass spectrum resulted from the average of 100 laser shots on the area of interest. Acquisition parameters were set as follows: reflector mode, positive polarity, acceleration voltage 20 kV, first grid voltage 60%, guide wire voltage 0.15%, extraction delay time 100 ns. MALDI analysis was performed with a saturated solution of α-cyano-4-hydroxycinnamic acid in a water and acetonitrile (1:1) containing 0.1% trifluoracetic acid.

Ion NIMS: the pulse primary ion source was angled at 45° to the sample and was operated at 25 kV beam energy, with primary ion dosage below static limit, a 50-ns pulse width and calibrated off hydrocarbon peaks. Secondary ions were electrically directed to the time-of-flight tube by a sample stage at ±2.5 kV and by an extraction lens oppositely biased at 4.5 kV.

NanoLC–ESI linear ion trap: nano-electrospray capillary columns (5 cm in length, 75 μm in inner diameter, containing 5-nm particles) tips were made in house with a P-100 laser puller (Sutter Instruments) packed with Zorbax SB-C_{18} stationary phase (Agilent). Water and acetonitrile (0.1% formic acid) were used as the mobile phases and the flow rate was $300\,nl\,min^{-1}$. The sample was loaded directly onto the capillary. The gradient went from 5% acetonitrile to 30% acetonitrile in 10 min, then to 98% acetonitrile over 35 min, held at 98% acetonitrile for 10 min, and finally maintained for 10 min before re-equilibration at 5% acetonitrile.

Peptide array and single cells. Peptides were printed onto the NIMS surface from 1:1 acetonitrile/water solution containing 0.1% trifluoracetic acid by using a custom arrayer with an ArrayIt contact printing head. BSA was reduced and alkylated before digestion. Cells were placed onto the NIMS surface with a micromanipulator and left to dry before mass analysis. After mass spectrometry analysis, cells were fixed with 2% paraformaldehyde and permeabilized with cold methanol. Blocking of non-specific binding sites was performed with 20% human AB serum before cells were indirectly immunofluorescently stained with a mouse monoclonal anti-Pan cytokeratin antibody and Alexa555 goat anti-mouse antibody along with a DAPI nuclear counterstain.

Metabolite extraction from cells. Cell lysate was extracted with 600 μl of 86% methanol/13% water/1% formic acid. Samples were sonicated for 20 min and subsequently transferred to 2-ml Eppendorf tubes. The samples were placed in the freezer at −20 °C and kept there for 60 min, after which they were centrifuged for 10 min in a 5417C centrifuge (Eppendorf) at 13,000 r.p.m.; the supernatant was decanted and dried before analysis.

Animals. C57Bl/6J mice were housed in ventilated cages in the Scripps Research Institute's vivarium, maintained on a 12-h dark/light cycle in a temperature- and humidity-controlled room. The care of the animals was in accord with the Lawrence Livermore National Laboratory (LLNL) Institutional Animal Care and Use Committee (IACUC) committee guidelines

Mouse embryo tissue slice preparation. Embryos were collected from pregnant dams at embryonic day 16.5, with the morning of vaginal plug detection designated embryonic day 0.5. Mice were deeply anaesthetized by isofluorane inhalation and killed by cervical dislocation. Embryos were collected, quickly frozen in OCT compound embedding medium (VWR International) on solid CO_2, equilibrated to −20 °C, sectioned at 12 μm and collected on the NIMS surface. Representative sections were collected on Superfrost Plus slides (Fisher Scientific) and stained with haematoxylin and eosin with routine histological techniques.

Blood and urine. Fresh urine and blood samples were spotted directly onto the NIMS surface without any further sample preparation. After 30 s, urine and blood drops were blown off with a nitrogen stream. For data processing of urine samples, all mass spectra were converted to ASCII text and imported into SpecAlign (http://physchem.ox.ac.uk/~jwong/specalign/) for baseline correction, normalization by total ion current and realignment/recalibration of individual spectra. For statistical analysis of codeine peak intensities, SigmaPlot 10 (Systat Software) was used.

Metabolite identification. Putative metabolites were identified on the basis of post-source decay fragment ions and the exact mass (*m/z*) by using the METLIN (http://metlin.scripps.edu/), Human Metabolome Project (http://redpoll.pharmacy.ualberta.ca/hmdb/HMDB/) and Lipid Maps (http://www.lipidmaps.org/) databases.